Spectral function for ^{4}He using the Chebyshev expansion in coupled-cluster theory

J. E. Sobczyk,[1] S. Bacca,[1,2] G. Hagen,[3,4] and T. Papenbrock[4,3]

[1]*Institut für Kernphysik and PRISMA$^+$ Cluster of Excellence, Johannes Gutenberg-Universität, 55128 Mainz, Germany*

[2]*Helmholtz-Institut Mainz, Johannes Gutenberg-Universität Mainz, D-55099 Mainz, Germany*

[3]*Physics Division, Oak Ridge National Laboratory, Oak Ridge, Tennessee 37831, USA*

[4]*Department of Physics and Astronomy, University of Tennessee, Knoxville, Tennessee 37996, USA*

(Received 12 May 2022; accepted 19 August 2022; published 19 September 2022)

We compute spectral function for ^{4}He by combining coupled-cluster theory with an expansion of integral transforms into Chebyshev polynomials. Our method allows us to estimate the uncertainty of spectral reconstruction. The properties of the Chebyshev polynomials make the procedure numerically stable and considerably lower in memory usage than the typically employed Lanczos algorithm. We benchmark our predictions with other calculations in the literature and with electron-scattering data in the quasi-elastic peak. The spectral function formalism allows one to extend *ab initio* lepton-nucleus cross sections into the relativistic regime. This makes it a promising tool for modeling this process at higher-energy transfers. The results we present open the door for studies of heavier nuclei, important for the neutrino oscillation programs.

DOI: 10.1103/PhysRevC.106.034310

I. INTRODUCTION

Lepton-nucleus cross sections are not only a invaluable tool to investigate the nuclear dynamics with clean electroweak probes [1] but have also become a hot topic in the short- and long-baseline neutrino programs aiming at extracting neutrino oscillation parameters [2–4]. Recently, we initiated a theory program that addresses low- and intermediate- energy lepton-nucleus scattering from first principles by combining the Lorentz-integral-transform with coupled-cluster theory (LIT-CC) to compute many-body response functions [5] and lepton-nucleus cross sections. In this approach, the final-state interaction is described consistently with the initial- state interaction by the same Hamiltonian rooted in quantum chromodynamics, see Refs. [6–8]. An example is the description of the longitudinal quasi-elastic peak of ^{40}Ca, see Ref. [8], and this paves the way for further investigations. Despite its success, this approach also has its limitations: the formalism is based on the nonrelativistic theory and at the moment is capable of predicting only inclusive cross sections. Efforts to include the spectrum of the outgoing nucleons below and above pion production are still lacking in *ab initio* calculations. Several other approximations and phenomenological methods instead offer a way to answer such questions [9–13], chief among them being the spectral functions formalism. While spectral functions can be computed phenomenologically [14–16], calculations were performed recently within the self-consistent Green's function (SCGF) method [17,18] using a similar Hamiltonian as in Ref. [8] for the initial state. In the past also the LIT method combined with hyperspherical harmonics was used to obtain the proton spectral function of ^{4}He [19].

The main advantage of the spectral function formalism lies in the possibility of detaching the high-energy physics from the ground-state properties of the nucleus under the assumption that the final-state interactions can be neglected. This not only allows one to make predictions for the quasi-elastic peak using the relativistic kinematics and currents, but this approach can also be used at higher energies, e.g., above the pion production threshold. Hence, developing efficient *ab initio* methods to compute spectral functions deserves attention, which goes beyond the mere fact that their calculation in a many-body system is *per se* an interesting and challenging task. In this work, we present an approach to the computation of spectral functions which opens up the possibility of using *ab initio* many-body methods in the high-energy regime.

The reconstruction of nuclear response functions requires information about the excited states of the system, but usually these are not easily accessible. To circumvent this issue, the problem has been often reformulated by computing integral transforms of the response function, with Lorentz and Laplace kernels being popular choices [20–24]. The computation of the integral transform requires one to (only) solve a bound-state problem. The inversion of the transform, needed to obtain the response function, has to be performed numerically. While accurate results have been obtained for a variety of electroweak observables [5,8,24–26], the inversion introduces an additional numerical error and is most stable when the response function exhibits only one or two broad peaks [27,28]. This scenario was recently explored using machine-learning techniques [29]. Spectral functions often have a more complicated structure and this makes the inversion of the integral transform difficult. Therefore, we propose here to use a different approach that is based on the Chebyshev expansion of the integral kernel (ChEK) introduced in Refs. [30,31]. Although it relies on the idea of the integral transform, it does not

 ©2022 American Physical Society

require its inversion. Moreover, for a given desired resolution of the spectral reconstruction it allows one to estimate an uncertainty.

The information about the (discrete) spectrum of excited states in a many-body system can be retrieved in various ways. The nuclear theory community is familiar with the Lanczos orthogonalization procedure [32], which for example is used in the LIT-CC method. An alternative approach, developed in the field of condensed-matter physics, is the kernel polynomial method (KPM) [33]. As for the KPM, the approach of this paper is also based on an expansion in Chebyshev polynomials.

This paper is organized as follows. In Sec. II, we review how the lepton-nucleus interaction in the quasi-elastic peak can be expressed in terms of spectral functions using the impulse approximation. In Sec. III, we present the theoretical framework for our calculations of spectral functions. We validate our method in ^{4}He, paying special attention to the center-of-mass problem in Sec. IV, and finally we conclude in Sec. V.

II. ELECTRON-NUCLEUS SCATTERING

Let us consider the process

$$e(k) + A(p_0) \to e'(k') + f(p_f), \tag{1}$$

where an incoming electron with four-momentum $k = (E_k, \mathbf{k})$ is scattered off a nucleus A, producing an outgoing electron with four-momentum $k' = (E'_k, \mathbf{k}')$ and a final (in general multiparticle) state f. The four-momentum transfer is $q \equiv (\omega, \mathbf{q}) = k - k'$. In the Born approximation, the electron interacts via the exchange of a single γ.

The inclusive cross section of this process can be written in terms of leptonic and hadronic tensors as

$$\frac{d\sigma}{d\omega d\cos\theta} = \left(\frac{\alpha}{q^2}\right)^2 \frac{|\mathbf{k}|}{|\mathbf{k}'|} L_{\mu\nu} W^{\mu\nu}, \tag{2}$$

with the angle of the outgoing lepton being θ, $\alpha \approx 1/137$, is the fine-structure constant. The lepton tensor is

$$L_{\mu\nu} = 2[k_\mu k'_\nu + k'_\mu k_\nu - g_{\mu\nu}(kk')]. \tag{3}$$

The nuclear structure information is encoded in the hadron tensor,

$$W^{\mu\nu} = \sum_f \delta^4(p_0 + q - p_f) \langle 0|(J^\mu)^\dagger|\Psi_f\rangle\langle\Psi_f|J^\nu|0\rangle, \tag{4}$$

where the current J^μ corresponds to the electromagnetic process.

In the following, we focus on the quasi-elastic mechanism, for which the interaction takes place on a single nucleon, kicking off a nucleon from the remaining $(A-1)$ nucleus in the final state. The electromagnetic current is a sum of one-body contributions, which in the second-quantization form is given by

$$J^\mu = \sum_{\alpha,\beta} \langle\beta|j^\mu|\alpha\rangle a^\dagger_\beta a_\alpha. \tag{5}$$

Here, the initial and final nucleon states are labeled by α and β, respectively. Within the spectral function formalism, we use the fully relativistic current in the matrix element treating the initial and final nucleons as free states

$$\langle p+q|j^\mu|p\rangle = \bar{u}(p+q) V^\mu u(p). \tag{6}$$

The current j^μ has a vector structure and u denotes a Dirac spinor. Constructing the most general form of V^μ using the available four-vectors, we have

$$V^\mu = F_1 \gamma^\mu + \frac{F_2}{2m} i\sigma^{\mu\nu} q_\nu. \tag{7}$$

We use $F_1^{n,p}$, $F_2^{n,p}$ parametrized as in Ref. [34].

The impulse approximation

At relatively large momentum transfer $\mathbf{q}$, one can assume that the struck nucleon is decoupled from the nuclear $(A-1)$ system, i.e., that the final-state interaction can be neglected. Within this impulse approximation, the final nuclear state factorizes as

$$|\Psi_f\rangle \longrightarrow a^\dagger_{p'}|\Psi_{A-1}\rangle, \tag{8}$$

where a plane-wave state $a_{p'}$ with momentum $\mathbf{p}'$ and energy $E_{p'}$ is added on top of the final $(A-1)$ system.[1] Using the current of Eq. (5), the one-body matrix element can be factorized as

$$\begin{aligned}
\langle\Psi_f|J^\mu|0\rangle &\to \sum_{\alpha,\beta} \langle\beta|j^\mu|\alpha\rangle\langle\Psi_{A-1}|a_{p'} a^\dagger_\beta a_\alpha|0\rangle \\
&= \sum_{\alpha,\beta} \langle\beta|j^\mu|\alpha\rangle\langle\Psi_{A-1}|\delta_{\beta p'} a_\alpha - a^\dagger_\beta a_{p'} a_\alpha|0\rangle \\
&\approx \sum_\alpha \langle p'|j^\mu|\alpha\rangle\langle\Psi_{A-1}|a_\alpha|0\rangle \\
&= \int \frac{d^3\mathbf{p}}{(2\pi)^3} \langle p'|j^\mu|p\rangle \sum_\alpha \langle\mathbf{p}|\alpha\rangle\langle\Psi_{A-1}|a_\alpha|0\rangle,
\end{aligned} \tag{9}$$

where the approximation in the third line assumes that the struck nucleon at the interaction vertex is exactly the one which is ejected from the nucleus [35] and in the last line we insert a complete set of states $\int d^3p/(2\pi)^3 |p\rangle\langle p|$. $\langle\mathbf{p}|\alpha\rangle$ are single-particle wave functions in momentum space. The process is shown schematically in Fig. 1.

The recoil energy $E_f^{\rm kin}$ of the $(A-1)$ system is negligible for heavy nuclei, and the excitation is given by the energy conservation

$$E_f^{A-1} = \omega + E_0 - E_{p'} - E_f^{\rm kin} \tag{10}$$

with the initial-state energy E_0.

[1] For simplicity we suppress spin and isospin indices.

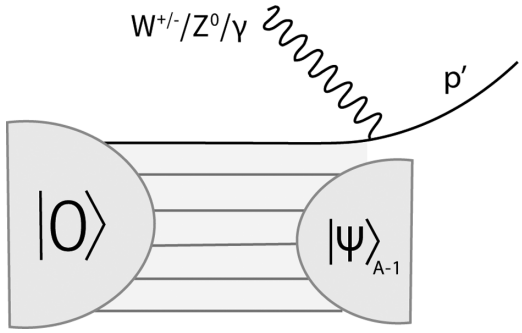

FIG. 1. Impulse approximation: the electroweak interaction takes place on a single nucleon which afterwards does not interact with the spectator $|\Psi_{A-1}\rangle$ system.

Substituting Eq. (9) in Eq. (4), the incoherent contribution to the hadron tensor becomes

$$W^{\mu\nu}(q) = \int \frac{d^3\mathbf{p}d^3\tilde{\mathbf{p}}}{(2\pi)^6} \sum_{\alpha,\alpha'} \sum\!\!\!\!\!\!\int_{\Psi_{A-1}} \langle p|(j^\mu)^\dagger|p'\rangle\langle p'|j^\nu|\tilde{p}\rangle \times \langle \mathbf{p}|\alpha\rangle^\dagger\langle\tilde{\mathbf{p}}|\alpha'\rangle\langle 0|a_\alpha^\dagger|\Psi_{A-1}\rangle\langle\Psi_{A-1}|a_{\alpha'}|0\rangle \times \delta\big(\omega - E_{p'} - E_f^{A-1} - E_f^{\rm kin} + E_0\big). \quad (11)$$

From the momentum conservation at the single nucleon vertex $\mathbf{p} = \tilde{\mathbf{p}} = \mathbf{p}' - \mathbf{q}$. Furthermore, the spin state of a_α and a'_α coincide due to charge conservation and the assumption that the nuclear ground state has spin zero. Finally, the last step of the factorization separates the energy conservation at the vertex from the excitation of the residual system by introducing the energy E needed to remove a nucleon with momentum $\mathbf{p}$ from the ground state as

$$\delta\big(\omega + E_0 - E_{p'} - E_f^{A-1} - E_f^{\rm kin}\big) = \int dE\,\delta\big(\omega + E - E_{p'} - E_f^{\rm kin}\big)\delta\big(E + E_f^{A-1} - E_0\big). \quad (12)$$

Using this equation and introducing explicitly the isospin dependence, the hadron tensor is

$$W^{\mu\nu}(q) = \int \frac{d^3\mathbf{p}}{(2\pi)^3} dE \big[S^n(\mathbf{p},E)w_n^{\mu\nu}(p,q) + S^p(\mathbf{p},E)w_p^{\mu\nu}(p,q)\big]\delta\big(\omega + E - E_{p+q} - E_f^{\rm kin}\big), \quad (13)$$

with $w_{n,p}^{\mu\nu}(p,q) = \langle p+q|j^\mu|p\rangle^\dagger\langle p+q|j^\nu|p\rangle$ depending on the isospin of $|p\rangle$, where we have introduced the hole spectral function

$$S^{n,p}(\mathbf{p},E) = \sum_{\alpha,\alpha'} \sum\!\!\!\!\!\!\int_{\Psi_{A-1}} |\langle 0|a_\alpha^\dagger|\Psi_{A-1}\rangle\langle\Psi_{A-1}|a_{\alpha'}|0\rangle \times \langle\mathbf{p}|\alpha\rangle^\dagger\langle\mathbf{p}|\alpha'\rangle\delta\big(E + E_f^{A-1} - E_0\big). \quad (14)$$

The spectral function gives the probability distribution of removing a nucleon with momentum $\mathbf{p}$ from the target nucleus, leaving the residual $(A-1)$ system with an energy $E_0 - E$. For closed-shell nuclei, such as the ^{4}He considered in this work, the spectral functions of spin-up and spin-down nucleons coincide. We normalize spectral functions as

$$\int \frac{d^3p}{(2\pi)^3} dE S^{n(p)}(\mathbf{p},E) = N(Z). \quad (15)$$

In the relativistic regimes, the factors m/E_p and m/E_{p+q} should be included to account for the implicit covariant normalization of the four-spinors of the nucleons in the matrix elements of the current j^μ. Hence the hadron tensor finally becomes

$$W^{\mu\nu}(q) = \int \frac{d^3\mathbf{p}}{(2\pi)^3} dE \frac{m}{E_p}\frac{m}{E_{p+q}} \times \big[S^n(\mathbf{p},E)w_n^{\mu\nu}(p,q) + S^p(\mathbf{p},E)w_p^{\mu\nu}(p,q)\big] \times \delta\big(\omega + E - E_{p+q} - E_f^{\rm kin}\big), \quad (16)$$

where one can see that it can be calculated starting from the spectral function for (n) neutrons and (p) protons.

We performed the factorization of the relativistic currents and the nuclear ground state governed by nonrelativistic dynamics. This way we can address the processes occurring at high energy-momentum transfers. This procedure introduces, however, some model dependence since we do not treat the wave function and the currents on an equal footing. In a consistent description we can either have the picture of a simple current interacting with a complicated nucleus, or an alternative picture (and a continuum of approaches between these two extremes) where the nucleus is simple (e.g., a product state), and the current is complicated and consists of one- and two-body terms. Very recently, authors of Ref. [36] presented a detailed discussion of this subject. In particular they analyze how the high-momentum behavior of the wave functions depends on the resolution of employed nuclear Hamiltonian. Their results can be applied to the momentum distribution of the spectral functions. We leave the analysis of this effect, as well the role of two-body currents within the factorization scheme, for the future studies.

III. FORMALISM

A. Green's function and spectral function

The spectral functions Eq. (14) are defined through the imaginary part of a propagator in a many-body system. Presently, we consider only the hole propagation of a state with quantum numbers α to a state with quantum numbers β:

$$G_h(\alpha,\beta,E) = \langle 0|a_\beta^\dagger \frac{1}{E - (E_0 - \hat{H}) - i\epsilon} a_\alpha|0\rangle,$$
$$\mathrm{Im}G_h(\alpha,\beta,E) = -\pi \sum\!\!\!\!\!\!\int_{\Psi_{A-1}} \langle 0|a_\beta^\dagger|\Psi_{A-1}\rangle \times \langle\Psi_{A-1}|a_\alpha|0\rangle\delta\{E - (E_0 - E_\Psi)\}. \quad (17)$$

The spectral functions can be retrieved from the imaginary part of Green's function summing over all appropriate quantum numbers:

$$S(\mathbf{p},E) = -\frac{1}{\pi}\sum_{\alpha,\beta}\langle\mathbf{p}|\alpha\rangle\langle\mathbf{p}|\beta\rangle^\dagger \mathrm{Im}G_h(\alpha,\beta,E). \quad (18)$$

The reconstruction of $\mathrm{Im}G_h(\alpha,\beta,E)$ from Eq. (17) requires a summation over all excited states $|\Psi_{A-1}\rangle$, which contains not only bound states but also continuum states. Within *ab initio* methods the calculated spectrum is typically discretized because of the truncation of the many-body space. Continuum effects can be included via complex-scaling techniques [37,38] or in the Berggren basis. The latter idea has been recently applied to obtain the microscopical optical potential from the coupled-cluster theory [39,40]. These techniques are usually combined with the Lanczos algorithm to construct tridiagonal forms of large matrices and thereby give access to the extreme eigenvalues of the problem. Here, however, we will use another approach described in the next section.

B. Chebyshev expansion of integral transform

Within the ChEK method we rephrase our problem: instead of reconstructing the response we want to estimate observables which are expressed as the energy integrals of the response. The method can be used in a general situation

$$\Phi = \int d\omega f(\omega) R(\omega), \tag{19}$$

where $f(\omega)$ is any bound function defining the observable and $R(\omega)$ is a response function—which in our case corresponds to $\mathrm{Im}G_h(\alpha,\beta,\omega)$. Our strategy to approximate the quantity in Eq. (19) consists in applying the integral transform $\tilde{R}(E)$:

$$\tilde{\Phi} = \int dE f(E)\tilde{R}(E), \tag{20}$$

in such a way that we control the approximation error $|\Phi - \tilde{\Phi}|$. Let us also notice that the reconstruction of Φ does not require the inversion of integral transform. In our case $\tilde{R}(E)$ is given by

$$\begin{aligned}\mathrm{Im}\tilde{G}_h(\alpha,\beta,E) &= \int d\omega \mathrm{Im}G_h(\alpha,\beta,\omega)K(\omega,E)\\ &= -\pi \sum\!\!\!\!\!\!\int_{\Psi_{A-1}} \langle 0|a_\beta^\dagger|K(E_\Psi, E-E_0)|a_\alpha|0\rangle\\ &= -\pi \langle 0|a_\beta^\dagger|K(\hat{H}, E-E_0)|a_\alpha|0\rangle. \end{aligned}\tag{21}$$

The kernel $K(\omega,E)$ can be realized by various functions. Here, we will apply the Gaussian kernel

$$K(\omega,E;\lambda) = \frac{1}{\sqrt{2\pi}\lambda}\exp\left(-\frac{(\omega-E)^2}{2\lambda^2}\right). \tag{22}$$

Following Ref. [30], we characterize the kernel as Σ accurate with Λ resolution:

$$\sup_{\omega_0\in[-1,1]} \sum\!\!\!\!\!\!\int_{\omega_0-\Lambda}^{\omega_0+\Lambda} K(\omega_0,E)dE \geqslant 1-\Sigma. \tag{23}$$

With these definitions we can provide the uncertainty bound for $|\Phi - \tilde{\Phi}|$, which depend on the properties of the function f and the kernel K.

Next we expand Eq. (21) into Chebyshev polynomials and truncate the number of terms N. This truncation will introduce an additional error, as will be explained later. The truncated kernel

$$K(\omega,E) = \sum_{k=0}^{N} c_k(E)\mathcal{T}_k(\omega) \tag{24}$$

is expressed in terms of $\mathcal{T}_k(\omega) = \cos[k\arccos(\omega)]$, which follow a recursive relation,

$$\begin{aligned}\mathcal{T}_0(x) = 1, \quad \mathcal{T}_{-1}(x) = \mathcal{T}_1(x) = x,\\ \mathcal{T}_{k+1}(x) = 2x\mathcal{T}_k(x) - \mathcal{T}_{k-1}(x).\end{aligned}\tag{25}$$

Let us assume that the Hamiltonian norm is known and that we are able to rescale our problem $[E_{\min}, E_{\max}] \to [-1,1]$. This allows us to use Chebyshev polynomials (which are defined on the interval $[-1,1]$). The Hamiltonian spectrum can be obtained, e.g., via the Lanczos algorithm. The rescaling is given then by

$$\begin{aligned}a = (E_{\max} - E_{\min})/2, \quad b = (E_{\max} + E_{\min})/2,\\ H := (H-b)/a.\end{aligned}\tag{26}$$

Combining Eqs. (21) and (24) we obtain

$$\begin{aligned}\mathrm{Im}\tilde{G}_h(\alpha,\beta,E) &= -\pi \sum_{k=0}^{N} c_k(E)\langle 0|a_\beta^\dagger \mathcal{T}_k(\hat{H})a_\alpha|0\rangle\\ &\equiv -\pi \sum_{k=0}^{N} c_k(E)\mu_k.\end{aligned}\tag{27}$$

For simplicity we abuse the notation and understand that $\mathrm{Im}\tilde{G}_h(\alpha,\beta,E)$ has an implicit N dependence. Furthermore, the moments μ_k have an implicit dependence on α and β. The moments of the expansion μ_k can be retrieved from a many-body calculation, using the recursive relation from Eq. (25):

$$\begin{aligned}\langle\tilde{\Psi}_0| &\equiv \langle 0|a_\beta^\dagger|, \quad |\Psi_0\rangle \equiv a_\alpha|0\rangle,\\ \langle\tilde{\Psi}_k| &\equiv \langle\tilde{\Psi}_{k-1}|\hat{H}|\Psi_k\rangle = \hat{H}|\Psi_{k-1}\rangle,\\ \mu_0 &= \langle\tilde{\Psi}_0|\Psi_0\rangle, \quad \mu_1 = \langle\tilde{\Psi}_0|\Psi_1\rangle \equiv \langle\tilde{\Psi}_1|\Psi_0\rangle,\\ \mu_{k+1} &= 2\langle\tilde{\Psi}_0|\Psi_{k+1}\rangle - \mu_{k-1} \equiv 2\langle\tilde{\Psi}_{k+1}|\Psi_0\rangle - \mu_{k-1}.\end{aligned}\tag{28}$$

In the $(k+1)$st step only the $|\Psi_k\rangle$ (or $\langle\tilde{\Psi}_k|$) state has to be known from the previous iteration. Similarly to the Lanczos procedure, we iterate the action of Hamiltonian $\hat{H}$. Here, however, no orthogonality restoration is needed at each step, which makes the procedure faster and requires less memory. The coefficients c_k from Eq. (27) depend on the chosen kernel and their form can be found in Ref. [31].

In the present case, we will define the function $f(\omega)$ in Eq. (19) as a histogram bin centered at η and a half width Δ

$$f(\omega) \equiv h_\Delta(\eta,\omega) = \begin{cases} 0 & |\eta-\omega| > \Delta \\ 1 & \text{otherwise.}\end{cases} \tag{29}$$

We are then interested in approximating the histogram,

$$\mathrm{Im}G_h(\alpha,\beta;\eta,\Delta) = \int h_\Delta(\eta,E)\mathrm{Im}G_h(\alpha,\beta,E)dE, \tag{30}$$

using its integral transform [given in Eq. (27)] with a finite number of Chebyshev moments N,

$$\mathrm{Im}\tilde{G}_h(\alpha,\beta;\eta,\Delta) = -\pi \sum_{k=0}^{N} \mu_k \int h_\Delta(\eta,E)c_k(E)dE. \quad (31)$$

As shown in Ref. [31], we get

$$\mathrm{Im}\tilde{G}_h(\Delta-\Lambda) - \Sigma - 2\gamma(\Delta-\Lambda) \leqslant \mathrm{Im}G_h(\Delta) \leqslant \mathrm{Im}\tilde{G}_h(\Delta+\Lambda) + \Sigma + 2\gamma(\Delta+\Lambda), \quad (32)$$

where we used a shorter notation $\mathrm{Im}G_h(\alpha,\beta;\eta,\Delta) \equiv \mathrm{Im}G_h(\Delta)$. The truncation error γ depends on the number of moments N and the properties of the kernel

$$\gamma = \sum_{k=N}^{\infty} c_k(E)\mathcal{T}_k(\omega). \quad (33)$$

The analytical expression for the bounds on γ can be found in Eqs. (B5) and (B22) of Ref. [31] for the Lorentzian and Gaussian kernels, respectively. As has been advocated in Ref. [31], the Gaussian integral transform has better convergence properties and will therefore be used in the present calculations.

Equation (32) is the master equation which will ultimately allow us to reconstruct the spectral functions defined in Eq. (18) as a histogram. It gives the error bound for $\mathrm{Im}G_h(\Delta)$ depending on the characteristics of the kernel, Λ and Σ, and the number of Chebyshev moments N [which enter both γ and $\mathrm{Im}\tilde{G}_h(\Delta\pm\Lambda)$].

It is important to notice some properties of the integral transform $\mathrm{Im}\tilde{G}_h(\Delta\pm\Lambda)$ [see Eq. (31)]. The characteristics of the kernel is encoded in coefficients c_k. In this way, the Chebyshev moments μ_k have to be calculated only once for any kernel to be used. This is an important feature, because their computation is much more expensive than the postprocessing stage (i.e., constructing histograms). Moreover, the integral of Eq. (31) can be performed analytically for the Gaussian kernel, which speeds up the calculation and does not introduce any additional numerical errors.

C. Coupled-cluster theory

The moments of the Chebyshev expansion μ_k in Eq. (28) have to be calculated in a many-body framework. In this work we employ the spherical coupled-cluster method [41], which can accurately describe ground- and excited-state properties of nuclei in the neighborhood of closed (sub-)shell nuclei. The method starts from a spherical Hartree-Fock reference state $|\Psi_{\mathrm{HF}}\rangle$ and includes correlations with an exponential ansatz

$$|0\rangle = e^T|\Psi_{\mathrm{HF}}\rangle. \quad (34)$$

Here the cluster operator T is built of 1p-1h, 2p-2h, ... excitations,

$$T = \sum_{i,a} t_i^a a_a^\dagger a_i + \frac{1}{4}\sum_{ijab} t_{ij}^{ab} a_a^\dagger a_b^\dagger a_i a_j + \cdots, \quad (35)$$

and is truncated at a certain level. In this work we truncate T at the 2p-2h excitation level, which is known as the coupled-cluster singles-and-doubles (CCSD) approximation.[2] The amplitudes t are obtained by solving a large set of coupled nonlinear equations, which are subsequently used in the construction of the similarity transformed Hamiltonian and creation and annihilation operators

$$\overline{H} = e^{-T}\hat{H}e^T, \quad \overline{a_\alpha} = e^{-T}a_\alpha e^T, \quad \overline{a_\alpha^\dagger} = e^{-T}a_\alpha^\dagger e^T. \quad (36)$$

For our problem, the initial states are built as

$$|\Psi_0\rangle = \overline{a_\alpha}|\Psi_{\mathrm{HF}}\rangle, \quad \langle\tilde{\Psi}_0| = \langle\Psi_{\mathrm{HF}}|\overline{a_\beta^\dagger}. \quad (37)$$

The calculation of Chebyshev moments follows Eq. (28), which requires iterating

$$|\Psi_k\rangle = \overline{H}|\Psi_{k-1}\rangle, \quad \langle\tilde{\Psi}_k| = \langle\tilde{\Psi}_{k-1}|\overline{H}. \quad (38)$$

The action of the Hamiltonian can be accumulated either on the right state, or on the left, or distributed between them. This allows for a numerical check of the procedure.

In our calculation we use the $\mathrm{NNLO_{sat}}$ nucleon-nucleon and three-nucleon interaction, which was adjusted to the binding energy and charge radii of light nuclei and selected oxygen isotopes [42]. Furthermore, we approximate the three-nucleon interaction at the normal-ordered two-body level which has been shown to be accurate for light- and medium-mass nuclei [43,44]. We note that this approximation breaks translational invariance of the Hamiltonian, and impacts the computation of intrinsic observables in light nuclei [45]. The results for various observables are converged in a model space of 15 oscillator shells ($N_{\max} = 14$) using the oscillator spacing $\hbar\omega = 16$ MeV. The three-nucleon interaction had an additional energy cut on allowed configurations given by $E_{3\max} = 16$ MeV.

IV. RESULTS

Before the analysis of the spectral function itself, we benchmark our result for the momentum distribution, which is directly derived from the spectral function:

$$n(\mathbf{p}) = \int dE S(\mathbf{p},E) = \sum_{\alpha,\beta}\langle\mathbf{p}|\alpha\rangle\langle\mathbf{p}|\beta\rangle^\dagger\langle 0|a_\beta^\dagger a_\alpha|0\rangle. \quad (39)$$

As coupled-cluster computations are performed in the laboratory system, one has to extract the intrinsic spatial density (or intrinsic momentum distribution) from the corresponding laboratory distributions. Within the coupled-cluster and in-medium similarity renormalization-group frameworks the nuclear ground-state has been shown to factorize with a very good precision into an intrinsic wave function and a Gaussian center-of-mass [46–48] when the kinetic energy of the center of mass is removed from the Hamiltonian. We note that this factorization was demonstrated in the coupled-cluster approach for a two-body Hamiltonian, while the in-medium similarity renormalization-group approach showed that this factorization holds when applying a three-nucleon interaction in the normal-ordered two-body approximation in nuclei as

[2] In Eq. (35) index a, b iterates over particle states, while i, j over hole states.

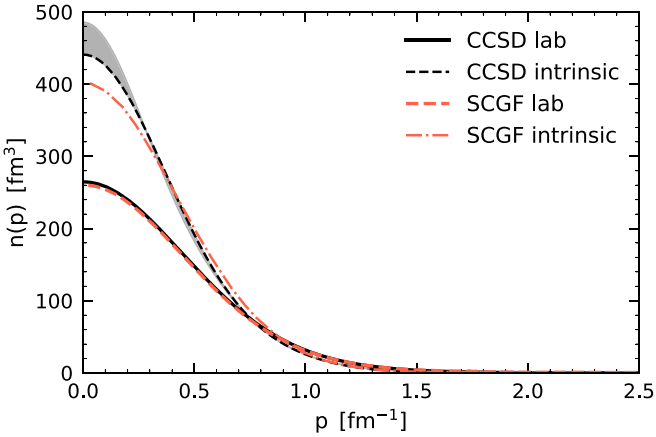

FIG. 2. Comparison of laboratory and intrinsic momentum distribution in ^{4}He (solid and dashed black lines). The gray band corresponds to an uncertainty of our procedure of removing the center-of-mass wave function. Results of SCGF [17] are shown for the laboratory (dashed line) and intrinsic momentum (dashed-dotted line). All the calculations were done with NNLO$_{\rm sat}$ interaction and the same model space.

light as ^{14}C [48]. Since the effect of breaking translational invariance was found to be small on the binding energy and radius of ^{4}He [42], we assume that factorization holds also for ^{4}He in the coupled-cluster theory. Assuming that the center of mass is a Gaussian, the extraction of intrinsic momentum distribution involves a deconvolution via Fourier transforms, and details are presented in the Appendix. Because of numerical reasons—varying the cutoff in the Fourier transform—the low-momentum region is affected by a few-percent uncertainty.

Figure 2 shows the intrinsic and laboratory proton momentum distributions computed within CCSD. The difference is clearly visible for low and intermediate momenta up to $k \approx 0.7$ fm^{-1}. We compare our results with those from the SCGF method. While the results coincide for the laboratory momentum distribution, there are visible differences to the intrinsic CCSD momentum density. We mostly ascribe them to two very different strategies of the center-of-mass removal. In our case the method is straightforward and relatively simple, while the procedure employed in Ref. [17] consists of two steps. First the SCGF result is approximated via an optimized reference state, then the center-of-mass component is removed from the wave function using Monte Carlo metropolis sampling. We note that the three-nucleon interaction is approximated slightly differently in the SCGF approach [49] and may therefore impact the comparison with our approach for intrinsic observables in ^{4}He. We speculate that this difference will lead to some discrepancies in the cross-section predictions. However, the low-momentum region plays a minor role since the hadron tensor is weighted by p^2dp [see Eq. (16)].

A. Spectral function

Benchmarking of the momentum distribution $n(\mathbf{p})$ allows us to validate the momentum dependence of the spectral function $S(\mathbf{p}, E)$ and compare it with a previous calculation of

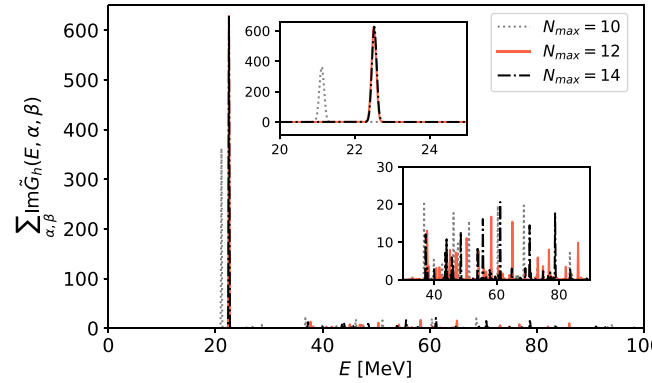

FIG. 3. The convergence of Gaussian integral transform of the proton Green's function $\sum_{\alpha,\beta} \mathrm{Im}\tilde{G}_h(\alpha, \beta, E)$. We applied the Gaussian kernel of width $\lambda = 0.0625$ MeV.

Ref. [17]. However, the spectral function energy dependence requires a more careful analysis. The energy distribution, driven by $\mathrm{Im}G(\alpha, \beta, E)$ is obtained via the integral transform expanded into Chebyshev polynomials. These are calculated according to recursive relations of Eq. (28) iterating the action of the Hamiltonian on the initial pivot state

$$|\Psi_n\rangle = \hat{H}^n|\Psi_0\rangle = \hat{H}^n a_\alpha|0\rangle. \tag{40}$$

Two remarks are in order. The initial state $|\Psi_0\rangle$ is composed of $(A-1)$ nucleons and, to be consistent, the Hamiltonian applied in the iteration should be changed accordingly. Otherwise the energy conservation of Eq. (17), $E_0 - E_\Psi$, would be shifted since E_Ψ is the excitation of the $(A-1)$ system. Additionally, $|\Psi_0\rangle$ might contain spurious center-of-mass excitations which should be detected and removed. The first point was already discussed in Refs. [39,50] and a method to account for this inconsistency was proposed. It consists in performing the calculation of the ground state and excitation energies both for A nucleons (E_0 and $\omega = E_0 - E_\psi$, accordingly) and $(A-1)$ (E_0^* and $\omega^* = E_0^* - E_\psi^*$, accordingly), so that we can calculate

$$E_0 - E_\Psi^* = E_0 - E_0^* + \omega^*. \tag{41}$$

We have checked that the difference between this value and $E_0 - E_\Psi$ is around 1.5 MeV. For the purposes of the spectral function—which is a valid approximation for the momentum transfer of several hundreds of MeV and energy transfers of tens of MeV—this difference is not drastic. It will be also partially taken into account since we consider spectral function in form of a histogram, whose binning will be larger than 1.5 MeV.

The disentanglement of the center of mass from the physical excitations in $\mathrm{Im}G(\alpha, \beta, E)$ is complicated. However, the spectral function of ^{4}He has a simple structure. It is dominated by a single peak whose position corresponds to the energy difference between the ground states of ^{4}He and ^{3}H (in the case of the proton spectral function) or ^{4}He and ^{3}He (in the case of the neutron spectral function). In Fig. 3, we show the Gaussian integral transform of the imaginary part of the Green's function of protons, $\sum_{\alpha,\beta} \mathrm{Im}\tilde{G}_h(\alpha, \beta, E)$, summed over all single-particle states. The dominant peak at around

22.5 MeV is converged already for $N_{\max} = 14$. It is shifted by 2.5 MeV with respect to the experimental value. This difference stems from the fact that we use the Hamiltonian of $A = 4$ for the system of $A - 1 = 3$ nucleons, as mentioned above. The smaller excitations visible at higher energies play a minor role. We also observe some very small contribution of states with negative strengths, which can be treated as unphysical excitations. We remove them from the final spectral function.

The analysis for ^{4}He shows that our treatment, although introducing some approximations, still gives reasonable spectral functions within a few percent of uncertainty. We were able to remove the center-of-mass contamination from the momentum-dependent part of the spectral function and performed various checks to make sure that the center-of-mass excitation does not strongly affect the energy distribution. For heavier nuclei the situation is known to be better, since center-of-mass effects scale as $1/A$.

To obtain the final spectral function within the ChEK method we need to know the scaling factors, see Eq. (26), which we estimate through the Lanczos algorithm, $E_{\min} = 0$ and $E_{\max} = 200$ MeV. The crucial part of the method is the choice of the binning when building a histogram on top of the discretized continuum states. There are at least two conditions that we want to fulfill:

(1) The first condition is imposed by the computational cost. We would like to keep the regularization width λ of the Gaussian kernel small (in the limit of $\lambda \to 0$ we would recover the eigenvalues of Hamiltonian). Knowing λ, we define the Λ-accurate kernel with Σ resolution [see Eq. (23)]. With this choice we can set Δ (binning width) to be large enough to minimize the reconstruction error in each bin. If we keep Σ and truncation error γ under control, then this error, given by Eq. (23) of the paper, will be mainly driven by

$$|\mathrm{Im}\tilde{G}_h(\Delta + \Lambda) - \mathrm{Im}\tilde{G}_h(\Delta - \Lambda)|. \qquad (42)$$

For the continuum spectrum, we can assume that the state density is uniformly distributed. In this case this error would be proportional to Λ/Δ.

In practice, especially when we apply the method to heavier systems, we are limited by the number of Chebyshev moments that we are able to calculate. In this situation, we would be forced to choose larger λ, and consequently Δ, in order to keep the reconstruction error low.

(2) Second, the number of discretized states in each bin has to be sufficiently large to mimic the continuum. The size of Hamiltonian in the space of 1h and 1p2h excitations for ^{4}He in our model space is of the order of 3000 (summed over isospin) and the spectrum is confined between (20,200) MeV. If we assume that the density of the spectrum is constant, then we can roughly estimate $3000/180 \approx 20$ states per 1 MeV. Therefore, we would choose bins of at least few-MeV width.

The density of states grows with the model space, with the order of expansion of the many-body method (e.g., adding triples to CCSD) and with the size of nucleus. In fact, for medium-mass nuclei we expect it to be high enough, so that the main challenge of the method would be to probe the spectrum with small enough λ.

Having in mind these above-mentioned conditions, we set the bin width to 3 MeV, because this is larger than the 2.5 MeV shift discussed earlier [see Eq. (41) and the discussion below]. We then use the Gaussian width $\lambda = 0.0625$ MeV and $\Lambda = 0.25$ MeV. According to the results of Ref. [31] the number of required moments would exceed $N = 10\,000$ to keep the truncation error below 1%. However, we numerically find that results are converged already with $N = 6000$ moments. With this choice of parameters we obtain a histogram for which the well-separated bound state is contained in one bin (of negligible error). The continuum spectrum binning is affected by an error of the order of $\Lambda/\Delta \approx 15\%$, which however does not impact the cross section due to its small contribution, see Fig. 3.

B. Electron-nucleus scattering

We now turn our attention to the electron scattering off ^{4}He. While we note that *ab initio* calculations of the ^{4}He electron-scattering cross section were already presented in Ref. [55] using a different Hamiltonian and including relativistic effects, here we want to focus on presenting our results and comparing them to an earlier calculation [17] that made use of the same Hamiltonian.

In Fig. 4, we show our results for the cross section in various kinematics, for the spectral function before and after removal of the center-of-mass contamination. The final results, "CCSD intrinsic," has been obtained by using the intrinsic momentum distribution. They predict more strength at the quasi-elastic peak with respect to the "CCSD laboratory" result. This trend is consistent with the findings of Ref. [17]. The uncertainty of $n(\mathbf{p})$ at low momenta as well as the negligible reconstruction errors coming from the ChEK method do not affect the cross-section results. It is also interesting to notice that the impulse-approximation indeed works better with increasing momentum transfer $|\mathbf{q}|$. For the values $|\mathbf{q}| \approx 300$–400 MeV the spectral function overestimates the data and predicts a shifted quasi-elastic peak.

A direct comparison of our results with Ref. [17] shows an overall good agreement. While the results before the center-of-mass removal are almost identical, the predicted cross section using the intrinsic spectral function is slightly different, as can be seen in Fig. 5. We have chosen this low momentum transfer kinematics, because the nuclear effects might play a more important role and differences between the CCSD and SCGF should be more pronounced. There are several sources of discrepancies. First, in the conservation of energy of Eq. (13) we take into account the kinetic energy of the recoiled nucleus, which for ^{4}He amounts to 7–9 MeV for the Fermi momentum. Second, we use a different approach to remove the center of mass. Third, the spectral functions are obtained using two different many-body methods and approximations therein.

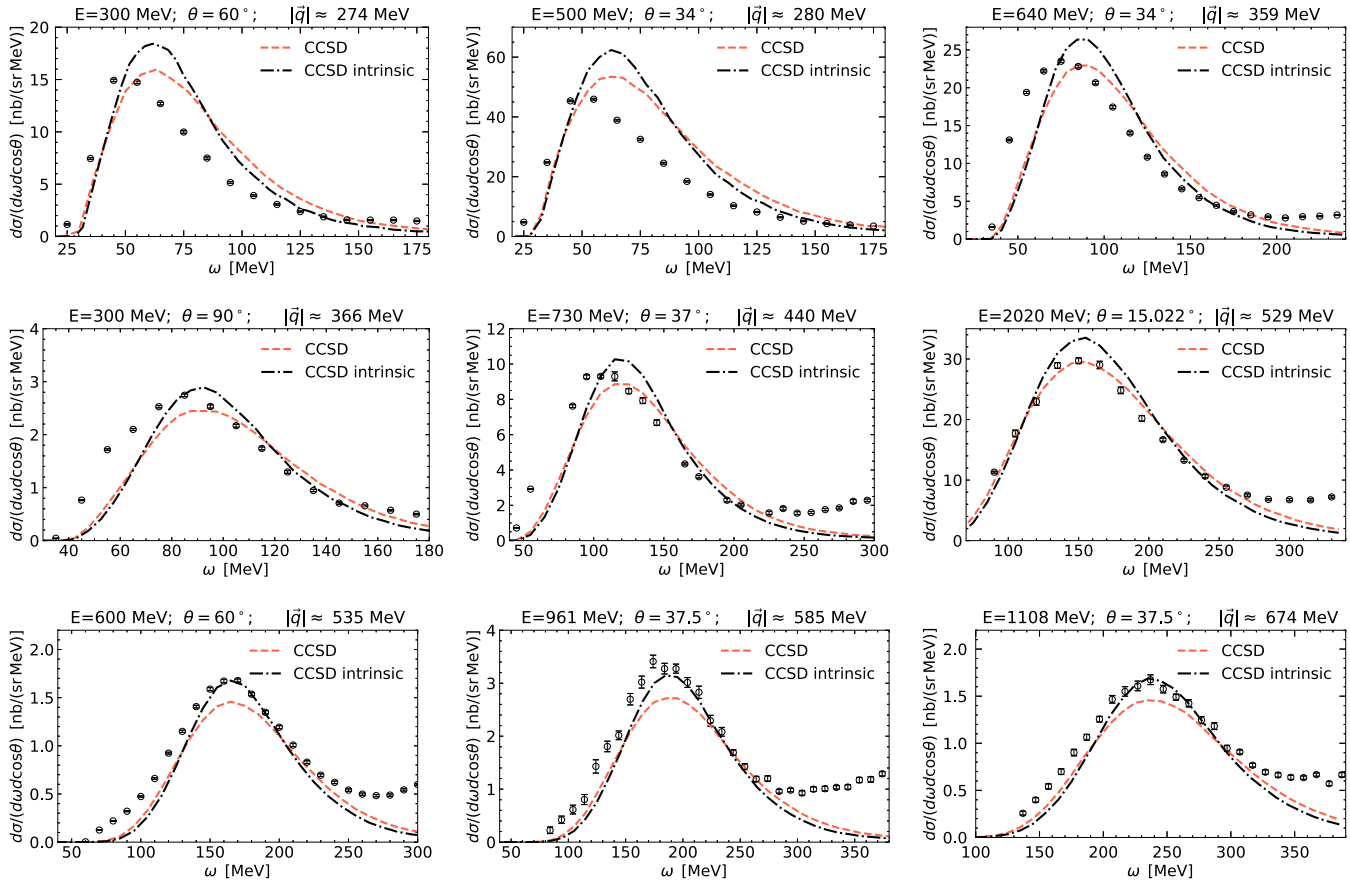

FIG. 4. Electron scattering on ^{4}He for different kinematics which correspond to the momentum transfers $|\mathbf{q}| \approx 270$–670 MeV. We show results obtained with CCSD before removing the center-of-mass contamination (dashed line) and afterwards, as explained in the main text (dashed-dotted line). Experimental data were taken from Refs. [51–54].

V. CONCLUSION AND OUTLOOK

We have presented an *ab initio* calculation of the spectral functions for ^{4}He based on the coupled cluster theory combined with the ChEK method for the reconstruction of the spectral properties of a many-body system. Within this approach, and for a given resolution, we were able to assess the uncertainty of our calculation. For ^{4}He we obtained an almost negligible error, however, we expect it to be larger when we move to medium-mass nuclei. This work paves the way for further explorations of the ChEK method in nuclear physics. On the one hand, one can study other nuclear responses, especially where the standard inversion procedures are unable to give stable results. On the other hand, the method provides error bounds, because it does not require any ansatz about the properties of the response (e.g., the threshold energy needed in the LIT inversion). This way we can achieve a stringent control over the uncertainty bound of an observable of interest.

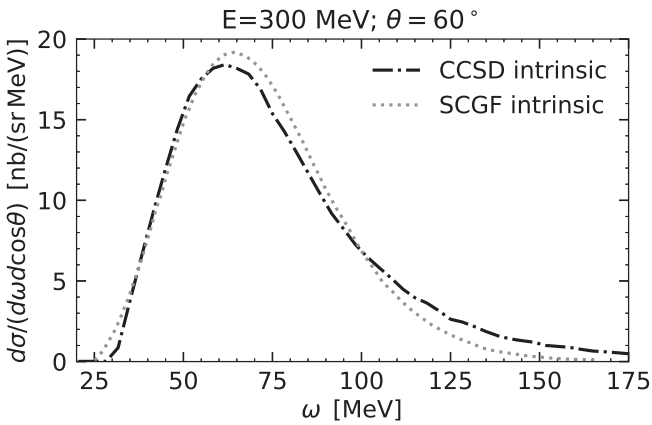

FIG. 5. Comparison of CCSD results with SCFG [17] on ^{4}He after removing the center-of-mass contamination.

We compared our predictions for the electron-nucleus scattering in the quasi-elastic regime with available data and found agreement. We were able to scan a large range of momentum transfers, and observed that the impulse approximation improves with growing momentum. Our results point to possible directions of further investigation. In view of the planned DUNE and T2HK experiments, which will benefit from reliable cross-section models, another important step is the calculation of spectral function for ^{16}O and ^{40}Ar. Both of these nuclei is within the reach of the coupled-cluster approach. Furthermore, for low and intermediate momentum transfers the impulse-approximation picture becomes less reliable and the full inclusion of final-state interactions is therefore

desirable. This transition region requires more theoretical studies as well as experimental data. Recent developments within coupled-cluster theory allow us to lead a consistent analysis based on the same many-body method, nuclear dynamics and truncations, employing both LIT-CC and spectral functions. Lastly, our approach does not presently account for two-body currents. Their role will also be a topic of our future work.

ACKNOWLEDGMENTS

We appreciate many illuminating discussions with A. Roggero. J.E.S. acknowledges the support of the Humboldt Foundation through a Humboldt Research Fellowship for Postdoctoral Researchers. This work was supported in part by the Deutsche Forschungsgemeinschaft (DFG) through the Cluster of Excellence "Precision Physics, Fundamental Interactions, and Structure of Matter" (PRISMA$^+$ EXC 2118/1) funded by the DFG within the German Excellence Strategy (Project ID 39083149). This material is based upon work supported by the U.S. Department of Energy, Office of Science, Office of Nuclear Physics under Award Nos. DE-FG02-96ER40963 and DE-SC0018223 (NUCLEI SciDAC-4 collaboration), and Contract No. DE-AC05-00OR22725 with UT-Battelle, LLC (Oak Ridge National Laboratory). Computer time was provided by the Innovative and Novel Computational Impact on Theory and Experiment (INCITE) program and by the supercomputer Mogon at Johannes Gutenberg Universität Mainz. This research used resources of the Oak Ridge Leadership Computing Facility located at Oak Ridge National Laboratory, which is supported by the Office of Science of the Department of Energy under Contract No. DE-AC05-00OR22725.

APPENDIX: REMOVAL OF THE CENTER OF MASS

We follow Ref. [56] and consider an A-body system with coordinates $\mathbf{r}_1, \ldots, \mathbf{r}_A$ and corresponding momenta $\mathbf{p}_1, \ldots, \mathbf{p}_A$ in the laboratory system. The center of mass and relative coordinates are

$$\begin{aligned}
\mathbf{R} &= \frac{1}{A}(\mathbf{r}_1 + \cdots + \mathbf{r}_A),\\
\boldsymbol{\xi}_1 &= \mathbf{r}_2 - \mathbf{r}_1,\\
\boldsymbol{\xi}_2 &= \mathbf{r}_3 - \frac{\mathbf{r}_1 + \mathbf{r}_2}{2},\\
&\vdots\\
\boldsymbol{\xi}_n &= \mathbf{r}_{n+1} - \frac{\mathbf{r}_1 + \mathbf{r}_2 + \cdots + \mathbf{r}_n}{n},\\
&\vdots\\
\boldsymbol{\xi}_{A-1} &= \mathbf{r}_A - \frac{\mathbf{r}_1 + \mathbf{r}_2 + \cdots + \mathbf{r}_{A-1}}{A-1},
\end{aligned} \tag{A1}$$

and the corresponding canonical momenta are

$$\begin{aligned}
\mathbf{P} &= \mathbf{p}_1 + \cdots + \mathbf{p}_A,\\
\boldsymbol{\pi}_1 &= \frac{\mathbf{p}_2 - \mathbf{r}_1}{2},\\
\boldsymbol{\pi}_2 &= \frac{2}{3}\mathbf{p}_3 - \frac{\mathbf{p}_1 + \mathbf{p}_2}{3},\\
&\vdots\\
\boldsymbol{\pi}_n &= \frac{n}{n+1}\mathbf{p}_{n+1} - \frac{\mathbf{p}_1 + \mathbf{p}_2 + \cdots + \mathbf{p}_n}{n+1},\\
&\vdots\\
\boldsymbol{\pi}_{A-1} &= \frac{A-1}{A}\mathbf{p}_A - \frac{\mathbf{p}_1 + \mathbf{p}_2 + \cdots + \mathbf{p}_{A-1}}{A}.
\end{aligned} \tag{A2}$$

Two comments are in order. First, the transformation between laboratory and center-of-mass coordinates has a unit Jacobian. Second, we see that $\boldsymbol{\xi}_n$ is the position of particle $(n+1)$ with respect to the center of mass of the previous n particles, while $\boldsymbol{\pi}_n$ is the momentum of particle $(n+1)$ relative to the average momentum of the $(n+1)$-particle system. We note that $\mathbf{r}_i - \mathbf{R}$ and $\mathbf{p}_i - \mathbf{P}/A$ are intrinsic positions and momenta, respectively, for any $i = 1, \ldots, A$. A particular convenient choice is $i = A$, because

$$\mathbf{r}_A - \mathbf{R} = \frac{A-1}{A}\boldsymbol{\xi}_{A-1}, \tag{A3}$$

$$\mathbf{p}_A - \frac{\mathbf{P}}{A} = \boldsymbol{\pi}_{A-1} \tag{A4}$$

can be expressed in terms of a single relative position and momentum, respectively.

Let us now assume that the ground state $|\Psi\rangle = |\Phi\rangle|\psi\rangle$ factorizes into a center-of-mass state $|\Phi\rangle$ and an intrinsic state $|\psi\rangle$. The laboratory density in position space is

$$\begin{aligned}
\rho(\mathbf{x}) &= A\int d^3\mathbf{r}_1 \cdots d^3\mathbf{r}_A \delta(\mathbf{x} - \mathbf{r}_A)|\Psi(\mathbf{r}_1, \ldots, \mathbf{r}_A)|^2\\
&= A\int d^3\mathbf{r}_1 \cdots d^3\mathbf{r}_{A-1}|\Psi(\mathbf{r}_1, \ldots, \mathbf{r}_{A-1}, \mathbf{x})|^2.
\end{aligned} \tag{A5}$$

Based on Eq. (A3), the intrinsic one-body density is

$$\begin{aligned}
\sigma(\mathbf{x}) &= A\int d^3\boldsymbol{\xi}_1 \cdots d^3\boldsymbol{\xi}_{A-1}\delta\left(\mathbf{x} - \frac{A-1}{A}\boldsymbol{\xi}_{A-1}\right)\\
&\quad \times |\psi(\boldsymbol{\xi}_1, \ldots, \boldsymbol{\xi}_{A-1})|^2\\
&= A\left(\frac{A}{A-1}\right)^3\int d^3\boldsymbol{\xi}_1 \cdots d^3\boldsymbol{\xi}_{A-2}\\
&\quad \times \left|\psi\left(\boldsymbol{\xi}_1, \ldots, \boldsymbol{\xi}_{A-2}, \frac{A}{A-1}\mathbf{x}\right)\right|^2.
\end{aligned} \tag{A6}$$

To establish the relation between the intrinsic and laboratory densities we use $\delta(\mathbf{x} - \mathbf{r}_A) = \delta(\mathbf{x} - \mathbf{R} - \boldsymbol{\xi}_{A-1}(A-1)/A)$ and rewrite Eq. (A5) as

$$\begin{aligned}
\rho(\mathbf{x}) &= A\int d^3\boldsymbol{\xi}_1 \cdots d^3\boldsymbol{\xi}_{A-1} d^3\mathbf{R}\,\delta\left(\mathbf{x} - \mathbf{R} - \frac{A-1}{A}\boldsymbol{\xi}_{A-1}\right)\\
&\quad \times |\Phi(\mathbf{R})|^2|\psi(\boldsymbol{\xi}_1, \ldots, \boldsymbol{\xi}_{A-1})|^2\\
&= \int d^3\mathbf{R}|\Phi(\mathbf{R})|^2\sigma(\mathbf{x} - \mathbf{R}).
\end{aligned} \tag{A7}$$

Thus, the laboratory density is a convolution of the center-of-mass density and the intrinsic density. In coupled-cluster and IMSRG calculations, the center-of-mass wave function is a Gaussian (to a very good approximation) [46–48,57,58], i.e.,

$$|\Phi(\mathbf{R})|^2 = \pi^{-3/2} b^{-3} e^{-\frac{\mathbf{R}^2}{b^2}}, \tag{A8}$$

and its Fourier transform is

$$(2\pi)^{-3/2} e^{-\frac{b^2}{4}\mathbf{P}^2}. \tag{A9}$$

Thus, the intrinsic density can be obtained by dividing the Fourier transforms of the laboratory and center-of-mass wave functions and performing the inverse Fourier transform of that quotient.

Let us now turn to momentum space. The laboratory momentum density is

$$\begin{aligned}\rho(\mathbf{p}) &= A \int d^3\mathbf{p}_1 \cdots d^3\mathbf{p}_A \delta(\mathbf{p} - \mathbf{p}_A) |\Psi(\mathbf{p}_1, \ldots, \mathbf{p}_A)|^2 \\ &= A \int d^3\mathbf{p}_1 \cdots d^3\mathbf{p}_{A-1} |\Psi(\mathbf{p}_1, \ldots, \mathbf{p}_{A-1}, \mathbf{p})|^2.\end{aligned} \tag{A10}$$

Based on Eq. (A4), the intrinsic one-body momentum density is

$$\begin{aligned}\sigma(\mathbf{p}) &= A \int d^3\boldsymbol{\pi}_1 \cdots d^3\boldsymbol{\pi}_{A-1} \delta(\mathbf{p} - \boldsymbol{\xi}_{A-1}) \\ &\quad \times |\psi(\boldsymbol{\pi}_1, \ldots, \boldsymbol{\pi}_{A-1})|^2 \\ &= A \int d^3\boldsymbol{\pi}_1 \cdots d^3\boldsymbol{\pi}_{A-2} |\psi(\boldsymbol{\pi}_1, \ldots, \boldsymbol{\pi}_{A-2}, \mathbf{p})|^2.\end{aligned} \tag{A11}$$

To establish the relation between the intrinsic and laboratory momentum densities we use $\delta(\mathbf{p} - \mathbf{p}_A) = \delta(\mathbf{p} - \boldsymbol{\pi}_{A-1} - \mathbf{P}/A)$ and rewrite Eq. (A10) as

$$\begin{aligned}\rho(\mathbf{p}) &= A \int d^3\boldsymbol{\pi}_1 \cdots d^3\boldsymbol{\pi}_{A-1} d^3\mathbf{P} \delta\left(\mathbf{p} - \boldsymbol{\pi}_{A-1} - \frac{\mathbf{P}}{A}\right) \\ &\quad \times |\Phi(\mathbf{P})|^2 |\psi(\boldsymbol{\pi}_1, \ldots, \boldsymbol{\pi}_{A-1})|^2 \\ &= \int d^3\mathbf{P} |\Phi(\mathbf{P})|^2 \sigma\left(\mathbf{p} - \frac{\mathbf{P}}{A}\right).\end{aligned} \tag{A12}$$

The substitution $\mathbf{K} = \mathbf{P}/A$ then yields

$$\rho(\mathbf{p}) = A^3 \int d^3\mathbf{K} |\Phi(A\mathbf{K})|^2 \sigma(\mathbf{p} - \mathbf{K}). \tag{A13}$$

Thus, the laboratory density is a convolution of the center-of-mass density (at A times its argument) and the intrinsic density. Again, the center-of-mass wave function is to a good approximation a Gaussian in momentum space, and the deconvolution can be performed. We have

$$A^3 |\Phi(A\mathbf{P})|^2 = \pi^{-3/2} b^3 A^3 e^{-b^2 A^2 \mathbf{P}^2}, \tag{A14}$$

and its Fourier transform is

$$(2\pi)^{-3/2} e^{-\frac{1}{4}\frac{\mathbf{R}^2}{A^2 b^2}}. \tag{A15}$$

In the Gaussians, we employed the oscillator length

$$b = \sqrt{\frac{\hbar}{M\tilde{\omega}}}. \tag{A16}$$

Here, $M = Am$ is the total mass in terms of the nucleon mass m, while $\tilde{\omega}$ is the frequency of the Gaussian; this parameter is independent of the oscillator basis, and we have $\hbar\tilde{\omega} \approx 24$ MeV for a light nucleus such as ^{4}He and $\hbar\tilde{\omega} \approx 16$–$20$ MeV for ^{16}O [46,47]. Thus $b \approx 0.7A^{-1/2}$ fm, and the Gaussian (A14) approximates a δ function for $A \gg 1$. We therefore expect that the difference between the laboratory and intrinsic density in momentum space becomes exponentially small for $A^{1/2} \gg 1$.

[1] S. Bacca and S. Pastore, Electromagnetic reactions on light nuclei, J. Phys. G **41**, 123002 (2014).

[2] L. Alvarez-Ruso *et al.* (NuSTEC Collaboration), NuSTEC White Paper: Status and challenges of neutrino-nucleus scattering, Prog. Part. Nucl. Phys. **100**, 1 (2018).

[3] A. M. Ankowski *et al.*, Electron scattering and neutrino physics, arXiv:2203.06853.

[4] L. A. Ruso *et al.*, Theoretical tools for neutrino scattering: interplay between lattice QCD, EFTs, nuclear physics, phenomenology, and neutrino event generators, arXiv:2203.09030.

[5] S. Bacca, N. Barnea, G. Hagen, G. Orlandini, and T. Papenbrock, First Principles Description of the Giant Dipole Resonance in ^{16}O, Phys. Rev. Lett. **111**, 122502 (2013).

[6] B. Acharya and S. Bacca, Neutrino-deuteron scattering: Uncertainty quantification and new $L_{1,A}$ constraints, Phys. Rev. C **101**, 015505 (2020).

[7] J. E. Sobczyk, B. Acharya, S. Bacca, and G. Hagen, Coulomb sum rule for ^{4}He and ^{16}O from coupled-cluster theory, Phys. Rev. C **102**, 064312 (2020).

[8] J. E. Sobczyk, B. Acharya, S. Bacca, and G. Hagen, *Ab initio* Computation of the Longitudinal Response Function in ^{40}Ca, Phys. Rev. Lett. **127**, 072501 (2021).

[9] J. Nieves, I. Ruiz Simo, and M. J. Vicente Vacas, Inclusive charged–current neutrino–nucleus reactions, Phys. Rev. C **83**, 045501 (2011).

[10] M. C. Martinez, P. Lava, N. Jachowicz, J. Ryckebusch, K. Vantournhout, and J. M. Udias, Relativistic models for quasi-elastic neutrino scattering, Phys. Rev. C **73**, 024607 (2006).

[11] J. E. Amaro, M. B. Barbaro, J. A. Caballero, T. W. Donnelly, A. Molinari, and I. Sick, Using electron scattering superscaling to predict charge-changing neutrino cross sections in nuclei, Phys. Rev. C **71**, 015501 (2005).

[12] T. Leitner, O. Buss, L. Alvarez-Ruso, and U. Mosel, Electron- and neutrino-nucleus scattering from the quasielastic to the resonance region, Phys. Rev. C **79**, 034601 (2009).

[13] O. Benhar, N. Farina, H. Nakamura, M. Sakuda, and R. Seki, Electron- and neutrino-nucleus scattering in the impulse approximation regime, Phys. Rev. D **72**, 053005 (2005).

[14] O. Benhar, A. Fabrocini, S. Fantoni, and I. Sick, Spectral function of finite nuclei and scattering of GeV electrons, Nucl. Phys. A **579**, 493 (1994).

[15] J. Nieves and J. E. Sobczyk, In medium dispersion relation effects in nuclear inclusive reactions at intermediate and low energies, Ann. Phys. (NY) **383**, 455 (2017).

[16] O. Buss, T. Leitner, U. Mosel, and L. Alvarez-Ruso, The influence of the nuclear medium on inclusive electron and neutrino scattering off nuclei, Phys. Rev. C **76**, 035502 (2007).

[17] N. Rocco and C. Barbieri, Inclusive electron-nucleus cross section within the self consistent Green's function approach, Phys. Rev. C **98**, 025501 (2018).

[18] C. Barbieri, N. Rocco, and V. Somà, Lepton scattering from ^{40}Ar and Ti in the quasielastic peak region, Phys. Rev. C **100**, 062501(R) (2019).

[19] V. D. Efros, W. Leidemann, and G. Orlandini, Exact ^{4}He spectral function in a semirealistic NN potential model, Phys. Rev. C **58**, 582 (1998).

[20] V. D. Efros, W. Leidemann, and G. Orlandini, Response functions from integral transforms with a Lorentz kernel, Phys. Lett. B **338**, 130 (1994).

[21] V. D. Efros, W. Leidemann, G. Orlandini, and N. Barnea, The Lorentz integral transform (LIT) method and its applications to perturbation-induced reactions, J. Phys. G **34**, R459 (2007).

[22] J. Carlson and R. Schiavilla, Euclidean Proton Response in Light Nuclei, Phys. Rev. Lett. **68**, 3682 (1992).

[23] J. Carlson, S. Gandolfi, F. Pederiva, S. C. Pieper, R. Schiavilla, K. E. Schmidt, and R. B. Wiringa, Quantum Monte Carlo methods for nuclear physics, Rev. Mod. Phys. **87**, 1067 (2015).

[24] A. Lovato, S. Gandolfi, J. Carlson, S. C. Pieper, and R. Schiavilla, Electromagnetic Response of ^{12}C: A First-Principles Calculation, Phys. Rev. Lett. **117**, 082501 (2016).

[25] S. Bacca, N. Barnea, G. Hagen, M. Miorelli, G. Orlandini, and T. Papenbrock, Giant and pigmy dipole resonances in ^{4}He, ^{16,22}O, and ^{40}Ca from chiral nucleon-nucleon interactions, Phys. Rev. C **90**, 064619 (2014).

[26] A. Lovato, J. Carlson, S. Gandolfi, N. Rocco, and R. Schiavilla, *Ab initio* Study of (ν_ℓ, ℓ^-) and $(\overline{\nu}_\ell, \ell^+)$ Inclusive Scattering in ^{12}C: Confronting the MiniBooNE and T2K CCQE Data, Phys. Rev. X **10**, 031068 (2020).

[27] S. Bacca, M. A. Marchisio, N. Barnea, W. Leidemann, and G. Orlandini, Microscopic Calculation of Six-Body Inelastic Reactions with Complete Final State Interaction: Photoabsorption of ^{6}He and ^{6}Li, Phys. Rev. Lett. **89**, 052502 (2002).

[28] S. Bacca, N. Barnea, W. Leidemann, and G. Orlandini, Effect of p-wave interaction in ^{6}He and ^{6}Li photoabsorption, Phys. Rev. C **69**, 057001 (2004).

[29] K. Raghavan, P. Balaprakash, A. Lovato, N. Rocco, and Stefan M. Wild, Machine-learning-based inversion of nuclear responses, Phys. Rev. C **103**, 035502 (2021).

[30] A. Roggero, Spectral density estimation with the Gaussian integral transform, Phys. Rev. A **102**, 022409 (2020).

[31] J. E. Sobczyk and A. Roggero, Spectral density reconstruction with Chebyshev polynomials, Phys. Rev. E **105**, 055310 (2022).

[32] C. Lanczos, An iteration method for the solution of the eigenvalue problem of linear differential and integral operators, J. Res. Natl. Bur. Stand. **45**, 255 (1950).

[33] A. Weiße, G. Wellein, A. Alvermann, and H. Fehske, The kernel polynomial method, Rev. Mod. Phys. **78**, 275 (2006).

[34] R. Bradford, A. Bodek, H. S. Budd, and J. Arrington, A new parameterization of the nucleon elastic form-factors, Nucl. Phys. B, Proc. Suppl. **159**, 127 (2006).

[35] W. H. Dickhoff and D. Van Neck, *Many-Body Theory Exposed!* (World Scientific, Singapore, 2005).

[36] A. J. Tropiano, S. K. Bogner, and R. J. Furnstahl, Short-range correlation physics at low renormalization group resolution, Phys. Rev. C **104**, 034311 (2021).

[37] R. Suzuki, T. Myo, and K. Kato, Level density in complex scaling method, AIP Conf. Proc. **768**, 455 (2005).

[38] J. Carbonell, A. Deltuva, A. C. Fonseca, and R. Lazauskas, Bound state techniques to solve the multiparticle scattering problem, Prog. Part. Nucl. Phys. **74**, 55 (2014).

[39] J. Rotureau, P. Danielewicz, G. Hagen, F. M. Nunes, and T. Papenbrock, Optical potential from first principles, Phys. Rev. C **95**, 024315 (2017).

[40] J. Rotureau, P. Danielewicz, G. Hagen, G. R. Jansen, and F. M. Nunes, Microscopic optical potentials for calcium isotopes, Phys. Rev. C **98**, 044625 (2018).

[41] G. Hagen, T. Papenbrock, M. Hjorth-Jensen, and D. J. Dean, Coupled-cluster computations of atomic nuclei, Rep. Prog. Phys. **77**, 096302 (2014).

[42] A. Ekström, G. R. Jansen, K. A. Wendt, G. Hagen, T. Papenbrock, B. D. Carlsson, C. Forssén, M. Hjorth-Jensen, P. Navrátil, and W. Nazarewicz, Accurate nuclear radii and binding energies from a chiral interaction, Phys. Rev. C **91**, 051301(R) (2015).

[43] G. Hagen, T. Papenbrock, D. J. Dean, A. Schwenk, A. Nogga, M. Włoch, and P. Piecuch, Coupled-cluster theory for three-body Hamiltonians, Phys. Rev. C **76**, 034302 (2007).

[44] R. Roth, S. Binder, K. Vobig, A. Calci, J. Langhammer, and P. Navrátil, Medium-Mass Nuclei with Normal-Ordered Chiral $NN+3N$ Interactions, Phys. Rev. Lett. **109**, 052501 (2012).

[45] T. Djärv, A. Ekström, C. Forssén, and G. R. Jansen, Normal-ordering approximations and translational (non)invariance, Phys. Rev. C **104**, 024324 (2021).

[46] G. Hagen, T. Papenbrock, and D. J. Dean, Solution of the Center-Of-Mass Problem in Nuclear Structure Calculations, Phys. Rev. Lett. **103**, 062503 (2009).

[47] G. Hagen, T. Papenbrock, D. J. Dean, and M. Hjorth-Jensen, Ab initio coupled-cluster approach to nuclear structure with modern nucleon-nucleon interactions, Phys. Rev. C **82**, 034330 (2010).

[48] N. M. Parzuchowski, S. R. Stroberg, P. Navrátil, H. Hergert, and S. K. Bogner, Ab initio electromagnetic observables with the in-medium similarity renormalization group, Phys. Rev. C **96**, 034324 (2017).

[49] A. Carbone, A. Cipollone, C. Barbieri, A. Rios, and A. Polls, Self-consistent Green's functions formalism with three-body interactions, Phys. Rev. C **88**, 054326 (2013).

[50] G. Hagen, T. Papenbrock, and M. Hjorth-Jensen, *Ab Initio* Computation of the F-17 Proton Halo State and Resonances in $A = 17$ Nuclei, Phys. Rev. Lett. **104**, 182501 (2010).

[51] J. S. O'Connell *et al.*, Electromagnetic excitation of the delta resonance in nuclei, Phys. Rev. C **35**, 1063 (1987).

[52] A. Zghiche *et al.*, Longitudinal and transverse responses in quasielastic electron scattering from ^{208}Pb and ^{4}He, Nucl. Phys. A **572**, 513 (1994).

[53] R. M. Sealock *et al.*, Electroexcitation of the Delta (1232) in Nuclei, Phys. Rev. Lett. **62**, 1350 (1989).

[54] D. B. Day *et al.*, Inclusive electron nucleus scattering at high momentum transfer, Phys. Rev. C **48**, 1849 (1993).

[55] N. Rocco, W. Leidemann, A. Lovato, and G. Orlandini, Relativistic effects in *ab initio* electron-nucleus scattering, Phys. Rev. C **97**, 055501 (2018).

[56] B. G. Giraud, Density functionals in the laboratory frame, Phys. Rev. C **77**, 014311 (2008).

[57] G. R. Jansen, Spherical coupled-cluster theory for open-shell nuclei, Phys. Rev. C **88**, 024305 (2013).

[58] T. D. Morris, N. M. Parzuchowski, and S. K. Bogner, Magnus expansion and in-medium similarity renormalization group, Phys. Rev. C **92**, 034331 (2015).